frontiers | Frontiers in Materials

TYPE Original Research
PUBLISHED 24 January 2024
DOI 10.3389/fmats.2024.1334863

OPEN ACCESS

EDITED BY
Wolfram Fürbeth,
DECHEMA Forschungsinstitut (DFI), Germany

REVIEWED BY
Shivshankar R. Mane,
National Chemical Laboratory (CSIR), India
Andres M. Durantini,
Southern Illinois University Edwardsville, United States

*CORRESPONDENCE
Christopher J. Barrett,
christopher.barrett@mcgill.ca

†These authors have contributed equally to this work and share first authorship

RECEIVED 07 November 2023
ACCEPTED 09 January 2024
PUBLISHED 24 January 2024

CITATION
Kim M, Hillel C, Edwards K, Borchers TH, Mermut O, Pietro WJ and Barrett CJ (2024), Azo dye polyelectrolyte multilayer films reversibly re-soluble with visible light. *Front. Mater.* 11:1334863. doi: 10.3389/fmats.2024.1334863

Azo dye polyelectrolyte multilayer films reversibly re-soluble with visible light

Mikhail Kim[1†], Coral Hillel[2†], Kayrel Edwards[1], Tristan H. Borchers[1], Ozzy Mermut[2,3,4], William J. Pietro[4] and Christopher J. Barrett[1,2*]

[1]Department of Chemistry, McGill University, Montreal, QC, Canada, [2]Department of Physics and Astronomy, York University, Toronto, ON, Canada, [3]Department of Electrical Engineering and Computer Science, York University, Toronto, ON, Canada, [4]Department of Chemistry, York University, Toronto, ON, Canada

Polymeric multilayer films were prepared using a layer-by-layer (LBL) technique on glass surfaces, by repeated and sequential dipping into dilute aqueous solutions of various combinations of water-soluble polyanions (polyacrylic acid (PAA)), polycations (polyallylamine hydrochloride (PAH) or chitosan (CS)), with bi-functional water-soluble cationic azo dyes bismark brown R bismarck brown red or bismark brown Y (BBY), or anionic azo dyes allura red (ALR) or amaranth (AMA), as ionic cross-linkers. The electrostatically-assembled ionically-paired films showed good long-term stability to dissolution, with no re-solubility in water. However, upon exposure to low power visible light under running water, the films photo-disassembled back to their water-soluble constituent components, via structural photo-isomerization of the azo ionic crosslinkers. The relative rate of the disassembly (RRD) of the films was established using UV-Vis spectroscopy, demonstrating that these assemblies can in principle represent fully recyclable, environmentally structurally degradable materials triggered by exposure to sunlight, with full recovery of starting components. A density functional theory treatment of the allura red azo dye rationalizes the geometrical isomerization mechanism of the photo-disassembly and provides insight into the energetics of the optically-induced structural changes that trigger the disassembly and recovery.

KEYWORDS

azo dyes, bioplastics, chitosan, light-responsive materials, photo-degradation

Introduction

Society's use of traditional disposable plastics has now clearly become a grave global environmental concern due to their overuse, non-degradability, poor processibility, and toxicity. In addition, plastic pollution creates enormous ecological, economic, and political problems (Shellenberger, 2020; Winch, 2020). However, encouraging efforts are being made in such fields as sustainable materials science and bioengineering towards providing low- or non-impact plastic alternatives using naturally derived polymers. From a chemical and engineering perspective, the design of plastics has two contrary goals: firstly to create materials that are durable, tough, and can be used for a long time, often requiring specific stability of use properties such as hydrophobicity, yet in contrast, an ideal material should

also be able to be recycled into new and fresh materials for re-use after disposal. In reality, the first goal of stability and longevity is achieved with oil-based materials held together with strong carbon-carbon covalent bonds, which precludes much ability to disassemble later, so the real efficiency of plastics recycling is currently still very low. Generally, less than 10% of plastic is recycled (Chamas et al., 2020) and the number of truly recyclable polymers is quite limited (Wunsch, 2000). Even for 'recyclable plastics', the process usually can be applied only one or two times, after which the plastic loses its integrity and/or depolymerizes. A promising solution is the use of environmentally biodegradable plastic in place of petroleum-based materials, however, the production of such bioplastics so far has been generally too expensive to be cost-competitive with oil-derived plastics. Environmental degradation of bioplastics can also still be quite slow to complete effectively after use (Zrimec et al., 2021), and the decay process can also begin while the material is still desired to be used, quite unfortunately. (Chinaglia et al., 2018).

An alternative approach is a plastic that can be reversibly assembled from non-toxic and/or highly recyclable parts into durable stable materials, and then under certain conditions (stimuli), reversible breaking of the bonds that hold the components together is triggered, leading to rapid and controlled disassembly of the plastic only on demand after use, back into their starting components without chemical degradation and ready for re-use. An example of such reversible assembly is to use 'soft' ionic bonds to hold the material together electrostatically, before triggering the process of disassembly, where the covalent bonds of each component remain intact and only soft bonds holding the constitutional parts together are released reversibly, with no harmful or useless by-products. After disassembly, the constitutional parts can then be re-incorporated completely into freshly-made re-assembled bioplastics, representing in principle a fully 100% recyclable, repeatable, and recoverable process with no environmentally harmful by-products. This provides the advantage of a material simultaneously being both biodegradable and reversibly-soluble. Previously described disassembled polymer systems utilized external stimuli such as change in temperature (Carl et al., 2019), change of pH (Cao and Wang, 2016), use of metal ions with chelating agents (Balkenende et al., 2014), mechanical force (Ayer et al., 2016), or UV-light (Ma et al., 2015; Ayer et al., 2016; Ji et al., 2021; Jung et al., 2021). Temperature, mechanical force, or UV light can however potentially lead to the decomposition of constitutional parts, and thus the effectiveness of recycling is diminished. The pH-responsive systems and systems utilizing metal ions and chelating agents also require a significant amount of aqueous solution of a strong acid or a base. This can also complicate the process of the disassembly as well as recovery of the constitutional parts and increase the cost prohibitively. Moreover, such approaches require complex synthesis, and the materials often exist only in the form of hydrogels, making it impossible to apply them as everyday-use materials to replace oil-based plastics, for example, as packaging materials.

In the work presented here, we propose using visible light as a clean, facile stimulus to trigger disassembly of water-insoluble materials made from water-soluble polyions and oppositely-charged water-soluble azobenzene dye ionic cross-linkers. Azobenzenes are a common class of inexpensive fabric dyes and food colourings which are well-known to isomerize upon visible light irradiation, changing their geometry and dipole moment significantly (Bandara and Burdette, 2012), (Figure 1). When bi-functional azo dyes are incorporated into ionic assemblies with polyelectrolytes as cross-linkers, this geometric photo-isomerization can be engineered to disrupt the ionic interaction between the polymer and azo dye significantly enough to photo-disassemble the material with low power visible light. The water-solubility of each component can then be recovered, completely unharmed and un-degraded in the process, for complete re-use. Previously, work using azo dye *trans*-to-*cis* photo-isomerization was shown to change the solubility of some compounds, for example, to enhance the aqueous solubility of an anti-cancer candidate drug in an aqueous environment (Ishikawa et al., 2017) and to release a drug from an azobenzene-polyethylene glycol-nanoparticle micelle system (Li et al., 2018). In other previous work (Borchers et al., 2021), co-crystallized halogen-bonding azo dyes with volatile components to yield materials that could be precisely cut, carved, or engraved with low-power visible laser light, releasing only the soft bonds holding the materials together, and returning the co-former components intact.

Applying visible light for disassembly materials was demonstrated previously (Xue et al., 2017; Tong et al., 2019) for some hydrogels or nanoparticles (Yang et al., 2013; Wang and Liao, 2016). An end-goal is to produce a free-standing plastic material, and to begin and better characterize our ionically assembled materials, we started with well-organized layer-by-layer (LbL) thin films on a transparent support surface, self-assembled as alternating layers of water-soluble polyions (such as polyacrylic acid (PAA), polyallylamine hydrochloride (PAH), and chitosan (CS)) and a variety of oppositely-charged bi-functional water-soluble azo dyes (bismarck brown Y (BBY), bismarck brown red (BBR), amaranth (AMA), and the most common food dye allura red (ALR)) held together via ion-ion interactions as cross-linkers. The chemical structures of these polymers and dye molecules are shown in Figures 2A, B, respectively. LbL assembly involves the sequential building of alternating layers of charged polymers/molecules from aqueous solution on a substrate via a spraying (Krogman et al., 2013) or dipping process of two water-soluble components, which after many layers results in a water-resistant thin film. Components are linked to each other in the films through soft, weak attractive forces such as electrostatic interactions, hydrogen bonding, or hydrophobic effects. Charged soft bonding interactions of polyanions and polycations, such as electrostatic interactions and hydrogen bonding, are of particular interest because both effects are easily reversible under gentle stimuli. This allows more complex systems to easily assemble and later reversibly disassemble when exposed to a particular stimulus such as pH, temperature, or salt, without breaking the covalent bonds of the individual component polymers. 'Green' aqueous-based LbL assembly offers many advantages compared to other traditional forms of film production, such as solvent casting, drop casting, and spin-coating; including ease of assembly with increased reproducibility, and a homogenous distribution of the components resulting in uniform films. LbL films and polyelectrolyte multilayer (PEM) films can be designed to be photo-responsive by: (i) covalently attaching a photo-switch to one of the polymers, or (ii) utilizing electrostatic interactions to crosslink the polymer using a photo-switchable

10.3389/fmats.2024.1334863

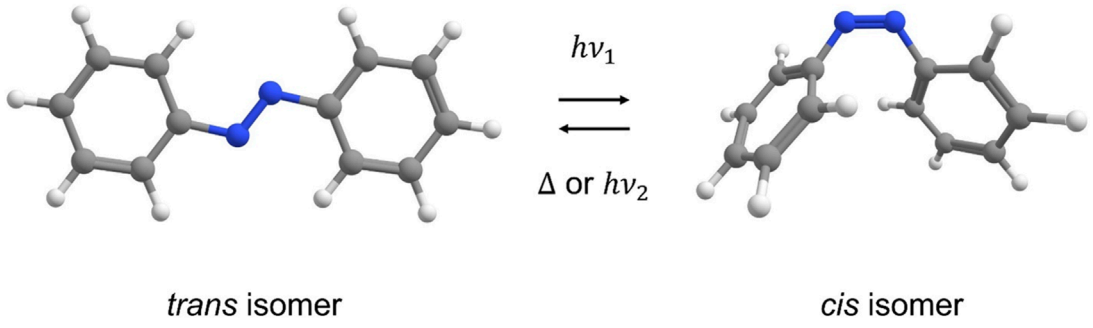

FIGURE 1
Reversible isomerization of azobenzene between stable *trans* and metastable *cis* isomers induced with light or heat.

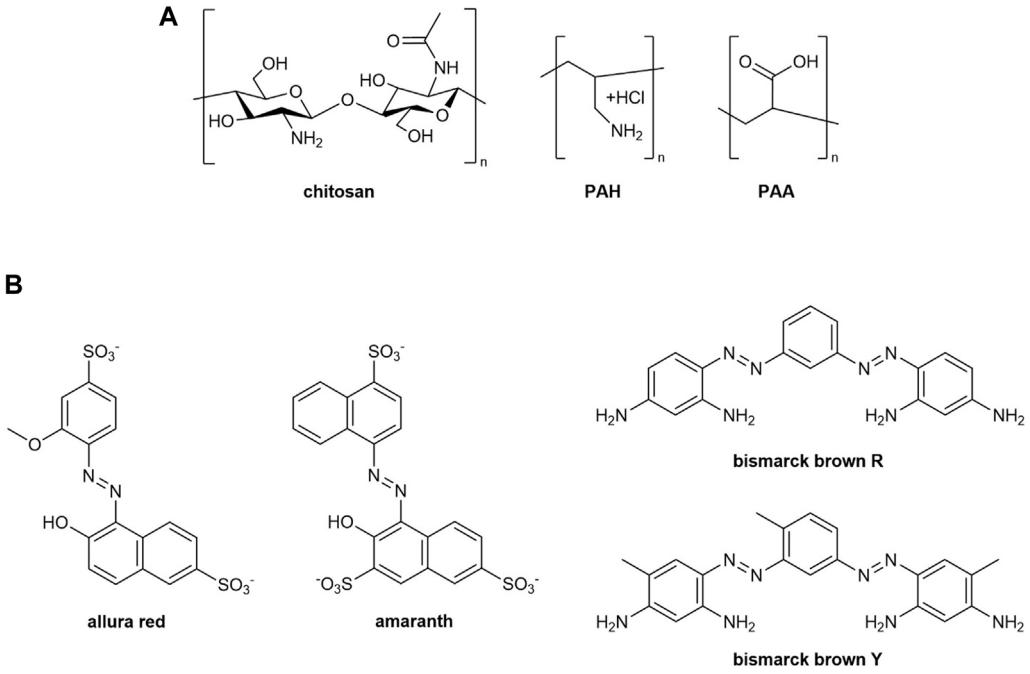

FIGURE 2
(A) Structures of polyelectrolytes used to assemble multilayer films, and **(B)** structures of azobenzene dyes used as ionic cross-linkers.

cross-linker molecule. For example, polyelectrolytes which have been covalently modified in this way include PAA, and silk fibroin modified with azo dyes, to be used as tunable extracellular matrix materials (Landry et al., 2017).

Light can be a preferred stimulus in comparison to non-optical stimuli since it can be applied precisely and remotely delivered with minimal undesired chemical change to the host materials. One of the most effective and well-studied photo-switches is azobenzene, which can photo-isomerize between *trans* and *cis* (E and Z) geometric isomers reversibly upon irradiation at their wide characteristic absorption band in their UV-Vis absorption spectra which originates from the π-π* transition of the chromophore. The azobenzene molecule can be easily functionalized to prepare a range of azobenzene-based (azo) dyes possessing various charged groups (Benkhaya et al., 2020). For example, many azo dyes FDA-approved as edible food colourings such as allura red and amaranth are negatively charged, and the water-soluble bismarck brown dyes, commonly used as histological stains, are positively charged. In a previous study, the kinetics of photo-switching of the bismarck brown Y (BBY) azo dye when crosslinked in layer-by-layer cellulose-based films was studied for the first time (Edwards et al., 2023), showing that the isomerization of these small molecules is still possible even when sandwiched between the polymer layers. The isomerization of azo dyes can result in large structural disruption, changing from a planar, nonpolar structure (*trans*) to a polar, twisted confirmation (*cis*). These changes on the molecular scale can result in large macroscopic changes in the entire material, and azobenzene-containing materials have

been developed for a wide variety of shape-changing applications, such as drug delivery via photo-driven assembly/disassembly, to fabricate surface relief holographic optical gratings, as sunlight-driven photo-actuators, and for photo-alignment of liquid crystal phases.

Generally, these materials are fabricated out of synthetic polymers. However, in response to the negative impact of synthetic polymers on the environment, a shift towards biodegradable and bio-based polymers has received much recent attention, and we have prepared electrostatically crosslinked LbL films for controlled photo-disassembly (Edwards et al., 2022), based on cellulose acetate (CA) and bismarck brown bi-functional azo dyes. Another non-toxic, cheap, and readily available biopolymer that can potentially replace petrol-based polymers such as PAA and PAH in these photo-reversible LbL materials is chitosan (CS), which is a positively charged, water-soluble, bio-based, and biodegradable polymer, and included in this report. CS is a linear polysaccharide constituted of repeating units of glucosamine and acetyl-glucosamine connected via a beta-1-4 linkage (Roberts, 1992) and is the deacetylated form of chitin, which is a biopolymer that can be ready extracted from the plentifully-available shells of crustaceans such as shrimp and lobster. Treatment of chitin with concentrated sodium hydroxide and mineral acid results in the production of biodegradable chitosan, commonly used in cosmetics, medicine (Yu et al., 2020), agriculture, and the food industry (Kean and Thanou, 2010; Siti Mohd Binti Isa and Mohamed, 2015). Previously, it was demonstrated that chitosan can be used in more advanced materials applications as multilayered films with copper ion detection properties (Borato et al., 2006), materials with optical storage capabilities (Dos Santos et al., 2003), hosting spontaneous birefringence (Sotero dos Santos et al., 2002), and as a controlled adsorption material (Tay et al., 2020).

In our current work, we extend from previous photo-degradable systems based on cellulose and bismarck brown azo dyes, now into readily-available and relatively harmless bifunctional azo-based food dyes (Silva et al., 2022) as the photo-addressable cross-linkers, paired with PAH and chitosan (Zhu et al., 2021) to produce a low-toxicity (in principle, even edible) light-responsive fully-recyclable material, with components whose environmental impact is greatly lessened. We report here the characterization of water-resistant self-assembled/disassembled multilayer polymer-azo dye materials, using a range of polyions for comparison (PAA, PAH, and bio-based CS) crosslinked using water-soluble azo dyes (BBR, BBY, and food dyes ALR, AMA) using the layer-by-layer technique. The multilayer thin films assembled were held together by electrostatic interactions between the oppositely charged polymer and photo-switch (azo dye) and provide a robust and stable material that was completely water resistant. Disassembly of these structured materials was triggered however by irradiation of visible light at sunlight intensities (~100 mW/cm^2) under a gentle flow of running water, disassembling the structure in reverse layer by layer, re-dissolving the materials back into their benign and non-toxic starting materials in a complete and controlled recycling process with, in principle, 100% recovery and re-use. A notable advantage is that this dis-assembly process can be accomplished with sunlight in environmental conditions, and thus represents a fully net-zero process energetically.

Materials and methods

LbL assembly of thin films

The chemical structures of the azo dyes and polymers used to prepare the multi-layered films are shown in Figures 2A, B. An automated slide stainer dipping robot Varistain 24–4 (Shandon Scientific Limited) was used to sequentially assemble multi-layered films consisting of the polymer crosslinked with the azo dyes (Figure 3A). For the substrate, 1″ × 3″microscope glass or quartz slides were cleaned by immersing in a 'piranha solution' (mixture of sulfuric acid/30% hydrogen peroxide) at room temperature for 24 h. For the systems involving anionic polymers and cationic azo dyes (e.g.,: PAA-BBR, PAA-BBY, CA-BBR, and CA-BBY) the multilayer deposition process was as follows: the negatively charged treated substrates were immersed in 0.01 M solutions of the positively charged cationic azo dye for 10 min, followed by three rounds of dipping in rinsing baths with deionized (DI) water (pH = 7) for 1 min each. The substrates were then immersed in the negatively charged polymer solutions (0.01 M of mers) for 10 min, followed by 3 similar rounds of 1 min rinsing with DI water. This dipping process was repeated to form a film with 50–90 bilayers (BL) in total. For the systems involving cationic polymers and anionic azo dyes (e.g.,: CS-AMA, CS-ALR, PAH-AMA and PAH-ALR), the multilayer deposition was analogous to the aforementioned process, however starting with dipping the negatively charged substrates into the positively charged polymer solution first, followed by washing and then immersion into the negatively charged azo dye solution. A schematic of the process of LbL assembly is shown in Figure 3A.

Light disassembly experiments

To mimic natural environmental degradation in the laboratory, 'sunlight and rainfall' conditions were simulated to examine the disassembly of the films by visible light, as depicted schematically in Figure 3B. The films deposited on glass and quartz substrates were clamped under a slow stream of DI water (pH = 7) with flow rate of 1–2 L/min maintained and recycled using an electric pump, at room temperature of approximately 20°C. The slides were mounted so that half the coated surface was shielded from light behind a black mask, but exposed to the same water flow, 'upstream' of the irradiated half of each slide. The black mask allowed for two zones of exposure, with the upper part of the slide being fully masked to prevent any exposure to light (control dark region), while the lower part of the slide was fully exposed to light irradiation. The films were irradiated using LEDs simulating sunlight spectra peaking in wavelengths either 380 nm, 460 nm, or 520 nm to match the azo absorption band, with light powers ranging from 10 mW to 5 W, placed 15 cm from the surface of the sample (Figure 3B). Such a distance provided irradiation for the experiment at intensities in the visible similar to sunlight, of up to 100 mW/cm^2, without heating the sample. For each series of experiments a thermometer was placed close to the sample under water flow to monitor the temperature change during the irradiation, and to confirm that the change in temperature in all experiments did not exceed ±0.5°C. For the negative control experiments, samples were left in running water

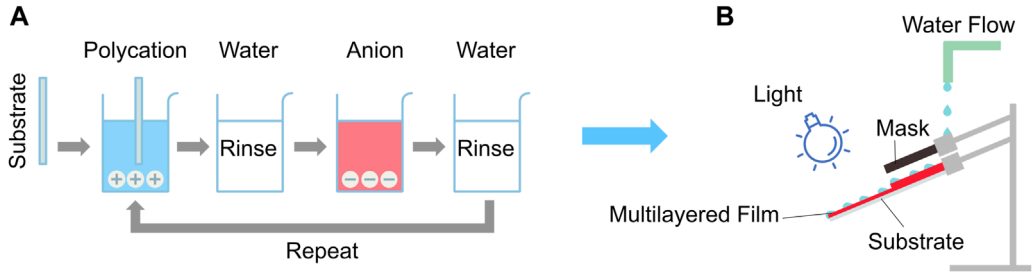

FIGURE 3
(A) Scheme of layer-by-layer (LbL) assembly for polymer-azo dye cross-linker multilayer films. **(B)** The experimental setup for light-disassembly of multilayered films under water flow in 'simulated sunlight and rainfall' environmental degradation conditions.

under ambient light for 2 days and no disassembly was observed either in the irradiated nor in the dark (mask-covered) regions. The UV-Vis absorption spectra of the coatings were recorded from 200 to 700 nm for quartz slides and 300–700 nm for glass slides. Photographs and UV-Vis measurements were taken at various time intervals, as shown in Figure 4, Supplementary Figure S2). The films were dried under a stream of air for 20 s before each measurement. These 'simulated sunlight and rainfall' experiments were performed in triplicate, and the disassembly rate was calculated from plots of absorbance vs. time. The loss of absorbance in the film was calibrated to diminishing film thickness using profilometry measurements in an atomic force microscope (AFM), as depicted in Figure 6.

Spectroscopies and analyses

UV-vis spectroscopy

UV–Vis spectroscopy of films was performed in transmittance mode using a Varian Cary 300 Bio spectrometer from Agilent Technologies, with a clean glass or quartz slide measured initially as background and also used during the measurements as the reference. UV-Vis absorption spectra of the coatings were recorded from 200 to 700 nm for quartz slides and 300–700 nm for glass slides in 2 nm increments. Prior to solution measurements, the UV-vis spectrum of a distilled water or a 1% water solution of acetic acid was measured as a background, and also used during the measurements as the reference.

To investigate the photo-bleaching behaviour of the azo dyes in different pH conditions upon irradiation by visible and UV light, 50 mL 0.1 M solution of each dye was prepared using distilled water, with the pH adjusted to pH = 4 using 0.1 M hydrochloric acid, or to pH = 12 using 0.1 M NaOH. 3 mL of each solution was placed in 3.5 mL 1 cm path length quartz cuvettes, closed and sealed with parafilm. The initial spectra of the solutions were collected and the cuvettes were placed in a gentle shaker 15 cm from the visible LED light source at either 460 nm (for ALR), or 523 nm (for AMA). For UV light, a mercury-vapor lamp was used, peaking near 360 nm. All measurements were conducted at ambient temperature of 20–22°C, and for each experiment a thermometer was placed inside another cuvette with the same solution and to confirm minimal temperature change during the shaking and irradiation, not exceeding 0.5°C.

FTIR, thermogravimetric (TGA), and differential scanning calorimetry (DSC) analysis

LbL films were carefully scraped from the surface of the substrate and ground to powder using an agate mortar. TGA of powder samples was performed before performing DSC experiments to determine temperature of destruction, on a Waters TA instruments Discovery 5,500 instrument in a nitrogen atmosphere. Average mass of the sample was 50 mg and the rate of heating was 10°C/min. DSC analysis was performed on Waters TA instruments Discovery 2,500 in a nitrogen atmosphere, heating from 0°C to 230°C, at a rate of 10°C/min, followed by cooling back down to 0°C from 230°C. The infrared (IR) spectra of the powder were acquired on a Perkin Elmer Spectrum II over the total range 4,000 cm^{-1} to 400 cm^{-1} at the best resolution 0.5 cm^{-1}, with a single bounce diamond attenuated total reflectance (ATR) accessory employed. The IR spectra were recorded in transmittance mode, averaged over 10 scans.

Atomic force microscopy (AFM)

AFM was used to determine the thickness of the films, measured as the change in height at the boundary of the masked region of the films, performed on a MFP3D AFM equipped with a molecular force probe controller (Asylum Research, Oxford Instruments) in AC mode in air using ACTA (AppNano) probes.

Computational chemistry

As the most common azo food dye and model system, optimized structures of ALR were calculated *in silico* using density functional theory (DFT) with the B3LYP functional (Lee et al., 1988; Becke, 1993) and ma-def2-TZVP basis set (Weigend and Ahlrichs, 2005; Zheng et al., 2011). To treat attractive Van der Waals interactions, Grimme's D3BJ dispersion correction was included in calculations (Grimme et al., 2010; Grimme et al., 2011). All calculations were performed in the Orca 5.0.3 software (Neese, 2012; Neese, 2017; Neese et al., 2020) with default settings, including the Resolution of Identity approximation (Weigend,

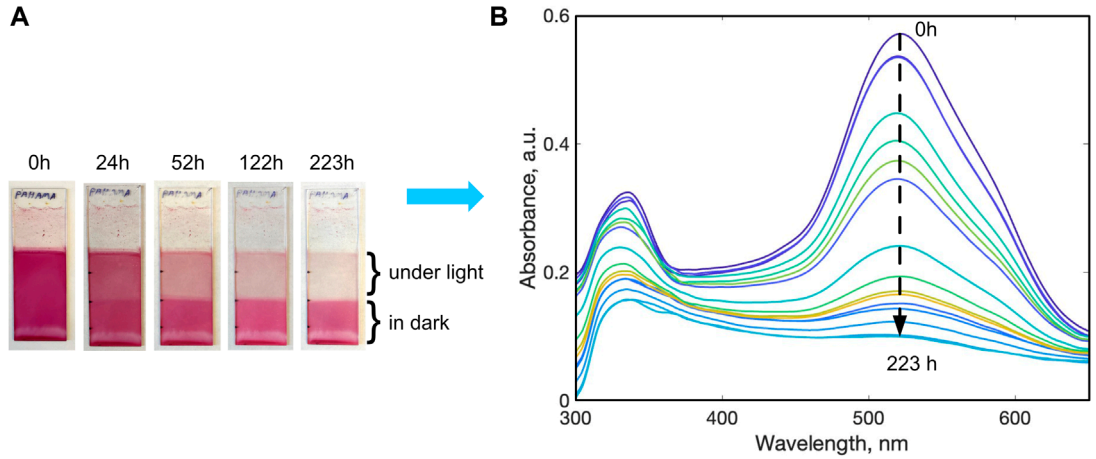

FIGURE 4
(A) Stages of light disassembly of a PAH-AMA multilayer film on a glass substrate, 90 BL, with 523 nm light irradiation, water flow rate 1.2 L/min, 25°C. **(B)** Change in the absorbance in the irradiated region during the disassembly process.

2002) with chain-of-spheres (RIJCOSX) (Neese et al., 2009; Izsák and Neese, 2011) and the def2/J auxiliary basis set (Weigend, 2006). Ground-state structures were verified by vibrational analysis (Bykov et al., 2015) and the absence of imaginary frequencies. Thermal *cis*-to-*trans* isomerization was investigated by a transition state search through the rotation pathway. This search was conducted by full geometry optimization under constraint of the CNNC dihedral angle, which was incremented in steps of 10°, with finer steps of 2.5° or less near the transition state. To reduce computation time, constrained optimizations were performed with the smaller basis set ma-def2-SVP (Weigend and Ahlrichs, 2005; Zheng et al., 2011), and then the energy of each structure along the reaction coordinate was evaluated as single points with ma-def2-TZVP. The identified transition state was further optimized with ma-def2-TZVP to estimate the activation barrier. Vibrational analysis of the transition state structure returned a single imaginary frequency corresponding to rotation about the azo-group.

Data processing and visualization

For data processing and visualization, MATLAB Version: 23.2.0.2391609 (R2023b) Update 2 was used. UV-vis and FTIR spectra were processed using 'Spectragryph' optical spectroscopy software. Molecular structures and vibrational modes from DFT were visualized with 'ChemCraft'.

Results and discussion

Multilayer films comprised of water-soluble polymers, both biodegradable cationic CS and synthetic polyelectrolytes (PAA and PAH) for comparison, were assembled using the LbL protocols described, with bi-functional photo-responsive crosslinker azo food-grade dyes ALR and AMA, and also with previously studied (non-food-grade) azo dyes BBY, BBR, again for comparison (Edwards et al., 2022). All combinations of these polymers and dyes produced robust and water-resistant materials that did not re-dissolve in water, over immersion periods of many months at ambient interior light intensity levels. In particular, this demonstrated that naturally-sourced CS biopolymer can form stable multilayer films similarly successful to their synthetic and non-bio-degradable counterparts PAH and PAA, two of the most common polyelectrolytes used in multilayer formation, and that non-toxic food dyes ALR and AMA can also be used as successfully stable cross-linker bi-anions, similar to BBY and BBR employed previously (Edwards et al., 2022). Under visible light irradiation at levels similar to strong exterior sunlight however, and the simulated environmental degradation conditions described, all multilayer films were observed to undergo gradual photo-driven disassembly while being gently washed with water under illumination. The systems PAH-ALR and PAH-AMA are described in this section in detail as best examples, and the analogous data and analysis are provided in the Supplementary Information SI for systems CS-ALR, CS-AMA, PAA-BBY, and PAA-BBR, to demonstrate that this photo-degradation can be a general phenomenon across a range of azo dyes and counter-polyelectrolytes. A full study of free-standing bioplastic materials of fully biodegradable food-grade CS-ALR and CS-AMA systems and their mechanical properties and similar photo-disassembly has been undertaken in parallel, and will be the subject of a forthcoming follow-up report.

The multilayer assemblies prepared were generally optically clear, with a deep red, pink, orange, or yellow appearance due to the characteristic colours of the green-, blue-, and violet-absorbing azo dyes used. For example, PAH-AMA coatings exhibited a deep pink colour (Figure 4B) while CS-ALR films exhibited a deep orange colour (Supplementary Figure S3A), similar to the spectra of the dyes employed in their assembly. UV-Vis absorption spectroscopy confirmed that the dye-polymer multilayers display a strong absorption band in the visible region (λ_{max} = 450–530 nm) ascribed to the π-π* azo transition (Figure 4B, S2A, S3A, S4A). As depicted in Figure 4B, UV-Vis absorption spectroscopy also displayed a broad

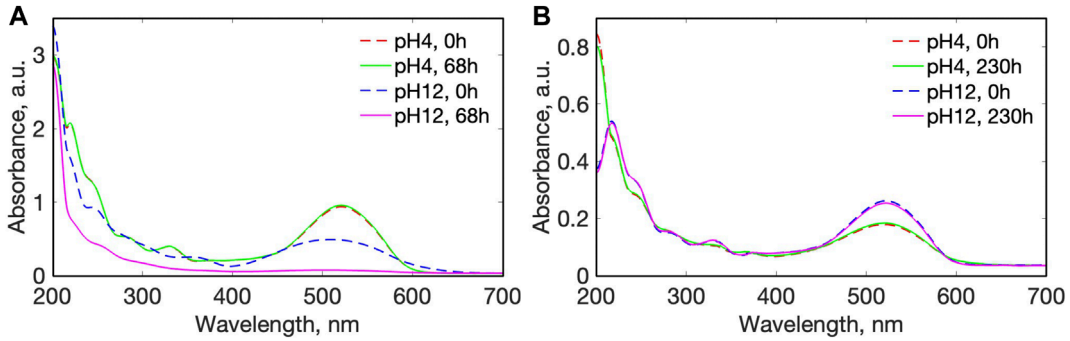

FIGURE 5
UV-Vis spectra of amaranth water solutions at pH = 4.0 and pH = 12.0 after exposure to: **(A)** UV light 300–390 nm, and **(B)** Green light (523 nm).

peak in the UV region ascribed to the n-π* transition of the azo dye and the characteristic peak associated with the polymers containing C–C bonds. The presence of electrostatic ionic interaction between the polymer and azo dye within the multilayered films was illustrated by FTIR spectroscopy, via the shifting peaks of sulpho-groups of the azo dyes from 1,010 to 1,020 cm^{-1} to 1,000 cm^{-1} and from 1,190 cm^{-1} to 1,170 cm^{-1} as shown in Supplementary Figure S5.

UV-vis spectroscopy

An advantage of using azo dyes as crosslinkers in these multilayered films is that their concentration within these materials can be readily tracked spectroscopically in real time, and therefore serve as a proxy for disassembly of the films layer-by-layer as the dye and polymer are released, according to Beer's Law. Complete recovery of the dye released from the assemblies into solution via the closed-loop washing cycle confirmed the non-degradation of the chromophores during the photo-disassembly process, which proves that this is a reversible physical disassembly only, and not a chemical degradation or bleaching of the dye. This is expected when using visible light at sunlight wavelengths and intensities only, as these dyes have been developed and long-used as stable, fast colourants for fabrics and food products. Using UV-Vis spectroscopy, the disassembly of the multilayered films was tracked over time as the films were exposed to various wavelengths and intensities of visible light, while being gently and constantly washed with water, to quantify the rate of photo-disassembly driven by the geometric *trans*-to-*cis* photo-isomerization of azo dyes BBY, BBR, AMA, and ALR.

It is proposed that during irradiation, the isomerization of the azo dyes within the multilayered films sufficiently disrupts the ionic interactions between polymer and the dye holding the material together, pairing the charges and thus keeping it water-resistant, and results in dissembling the multilayer structures back into their water-soluble starting components. Visually, a decrease of optical colour intensity in the irradiated part of the films was observed, as shown, for example, in Figure 4A. To quantify this disassembly process, UV-Vis spectroscopy was used to monitor the decrease in the absorbance (and thus dye concentration) of the large absorption peaks in the visible region corresponding to π-π* electronic transition of the–N=N–bonds, by recording absorbance change with time, as shown in Figure 4B.

To demonstrate that the disassembly of the materials was due to both removal of the azo dye and the polymer from the substrate over time, the multilayered films were also prepared on quartz substrates in addition to glass. Glass absorbs in the UV-B and UV-C region and precludes monitoring of the absorbance bands characteristic of all the polymers used for assembly (such as near λ = 200–220 nm), yet quartz substrates however do not absorb in this UV region and thus permit spectral peaks of just the polymers to be collected. Time-dependent UV-Vis spectra of the multilayer films on quartz substrate for system PAH-ALR showed the decrease in absorption peak of the polymer (λ ~ 210 nm) during disassembly experiments, concomitant with the decrease of the dye observed in the visible region. This confirmed that the polymer disassembles at similar rates to the dye disassembling, yet the multilayer films prepared on the quartz substrates were not as uniform or reproducibly good quality as those prepared on glass, possibly due to the quartz surfaces possessing fewer charged groups on the surface compared to glass, and/or less roughness, so glass was chosen as the preferred substrate for all experiments except for the UV absorbance of the polymer components.

In order to prove that the disassembly under light was not due to the photobleaching of the azo dye (decomposing of the organic compound due to high light energy), we compared UV-Vis spectra of acidic and basic water solutions at two extreme conditions of disassembly of AMA after exposure to both high-power UV light and to low-power green light (Figure 5). After 5W exposure of UV light to solutions at pH = 4.0, the spectra of the azo dye did not change significantly even after 68 h of irradiation (Figure 5A) confirming no chemical destruction of the dye. However, at a basic pH = 12.0 the main peak at 520 nm decreased dramatically after 68 h of exposure indicating degradation of the azo dye, in agreement with a previous stability assessment (Si et al., 2021). Hence, the spectra of the induced photo-degradation process by UV light in basic solution was used as a positive control for photo-bleaching. For the azo dyes used in this study, the wavelength of light required to initiate *trans*-to-*cis* photo-isomerization was in the visible range of blue-green light (460–532 nm), so low powered (8 mW) green LED lights were used. Spectra of the azo dyes in both acidic and

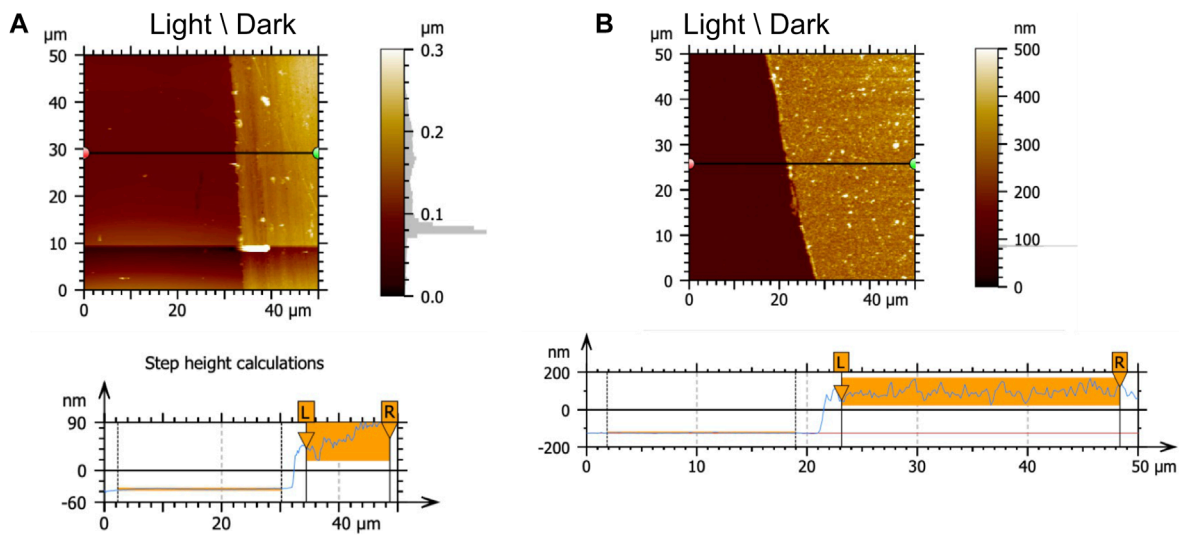

FIGURE 6
Determination by AFM of the thickness of **(A)** PAH-AMA multilayer film (80BL) deposited on a glass substrate, thin film (yellow) on a glass substrate (red), thickness 84 nm. **(B)** PAA-BBY multilayer (70BL) deposited on glass substrate, thin film (yellow) onto on glass substrate (red), thickness 204 nm. Data processed using Mountains SPIP v. 9.1.9837 (digital Surf). Scan specs: resolution (512 × 512), Scan rate (0.5 Hz and 1.0 Hz), scan size 5–50 μm.

basic solutions (Figure 5B) even after 231 h of exposure to low-power green light did not change significantly, confirming that any decrease in their absorbance over time and/or disassembly of the multilayer films, was not due to the chemical destruction of the azo dye. As a further control, multilayer films comprised of CS-PAA, and PAH-PAA did not show any degradation of disassembly under similar irradiation, confirming that the presence of the azo dye as cross-linker is essential to disassembly.

Physical properties of the LbL films (AFM, TGA, DSC)

The thermo-mechanical characteristics of the multilayer films were determined by TGA and DSC, where it was observed that the systems containing the azo dyes had a higher thermal decomposition temperature and glass transition temperature than their components (Supplementary Figure S6). The *Tg* of both the PAH-AMA and CS-AMA systems was observed to be between 180°C and 185°C, in comparison to *Tg* values of ~10°C and ~85°C for PAH and CS respectively. To confirm that the decrease in optical absorbance corresponded to a decrease in the thickness of the films, the thickness of the 4 multilayer systems was measured directly by profiling with AFM, at the region of height transition from the masked to the un-masked regions. Two examples of this thickness-loss confirmation are shown in Figure 6, for a PAH-AMA 80 bilayer film 84 nm thick, and a PAA-BBY 70 bilayer film 204 nm thick, both reduced to bare substrate (thickness = 0) in the irradiated regions.

DSC has confirmed that the *Tg* of PAA is of the order of 103°C and increases with increasing anhydride content, reaching a value (extrapolated) of 140°C for the pure linear anhydride (Eisenberg et al., 1969). The *Tg* of cellulose powder was reported to be in range 200–250°C, close to the temperature of initial decomposition of 266°C (Karing et al., 1960). In Szcześniak et al. (2007) it was shown that the *Tg* of cellulose depends on the degree of crystallinity and water content inside the polymer and can vary from −40–230°C. A similar biopolymer, gelatin, has a *Tg* around 60°C which can be increased with increased degree of inter- and intramolecular cross-linking (Perkasa et al., 2013). The *Tg* of chitosan can vary from 150 to 160°C, depending mostly on the water content inside the polymer and less so on the degree of acetylation (Dong et al., 2004). Observed increases of *Tg* of polymer-azo dye systems can be rationalized by considering the increased number of inter- and intramolecular cross-links between the polymers by azo dyes. In case of chitosan, the interaction between the biopolymer and azo dye can also lead to change in the degree of crystallinity, resulting in the higher *Tg* than for the pure polymer.

Assessing disassembly of multilayer films

Complete dye recovery with no chemical damage was confirmed by collection and analysis of the coloured rinse bath water. With confirmation by AFM and quartz UV-Vis analysis that the optical absorbance decreases are accompanied by a removal of the polymer and a decrease in the multilayer thickness, UV-Vis spectrophotometry could thus be employed to readily monitor the disassembly of the films and with confidence, in real time, under irradiation. Figure 4A shows qualitative photographs of a PAH-AMA film which was initially a deep pink color, which fully diminishes after 233 h of continuous irradiation with green light in the un-masked region, while being gently washed with water. The associated set of time-dependent UV-Vis spectra presented in Figure 4B quantifies that with this decrease in the colour of the film, the absorbance decreased from 0.6 to 0.1, at the ~520 nm peak corresponding to the AMA azo dye π-π* transition, as the concentration of the azo dye on the substrate

10.3389/fmats.2024.1334863

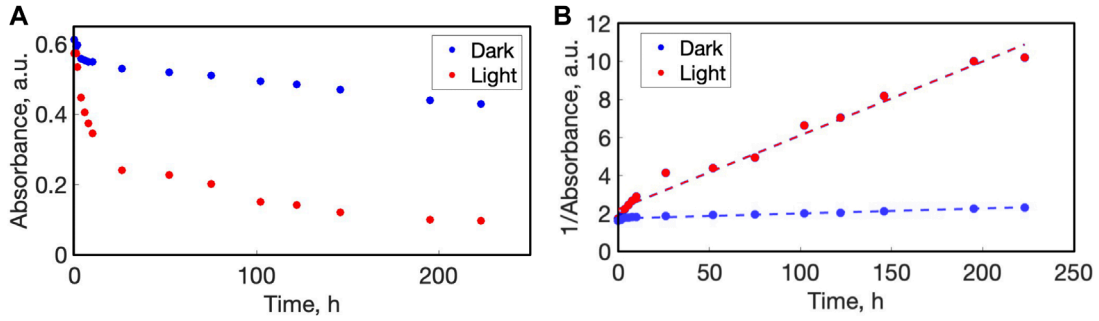

FIGURE 7
(A) Change in the absorbance maxima of PAH-amaranth multilayer films over time of disassembly (90 BL, 523 nm light). **(B)** Linearized data of change in the 1/absorbance maxima of the amaranth in multilayer film PAH-AMA for determination of the rate of the disassembly.

decreased towards zero. Similarly, Supplementary Figure S1 shows corresponding photographs of the multilayer films of (A) PAA-ALR, (B) CS-ALR, and (C) PAA-BBY over time with irradiation of light, while being gently washed with water, to 367 h, 141 h, and 50 h respectively. Supplementary Figure S2 quantifies the time dependent UV-Vis spectra band decreases for the PAH-ALR films, which similar to the PAH-AMA films, shows that during irradiation there was a decrease in the absorbance at ~ 490 nm (the π-π* transition for ALR) from absorbance 0.8 to 0.1, as the concentration of the azo dye in the remaining multilayer decreased towards zero.

To calculate a relative rate of disassembly (RRD), the absorbance at the azo dyes λ_{max} was plotted over time, as shown in Figure 7 for PAH-AMA, and in Supplementary Figure S2–4 (parts B) for the systems PAH-ALR, CS-ALR, and PAA-BBY. For the PAH-AMA system it was observed that the initial absorbance varied somewhat on x-y position, due to a slightly uneven distribution of the thickness of films, as in general such LbL films assembled vertically by robots tend to be thicker near the bottom due to adsorption-gravity gradients. In both the irradiated and un-irradiated ('light', red points; and 'dark', blue points) regions of the film, an initial steep decrease of the absorbance is generally observed. For both light and dark areas, this initial decrease is attributed to the leaching out of the films of excess dye that was not fully ionically adhered and remained un-washed away during fabrication in the relatively brief rinsing cycles.

To quantify a rate of disassembly the, absorbance (A) was plotted against time in the following coordinates: *1/A* vs. *time* and *lnA* vs. *time*, with the R-squared values of *1/A* vs. *time* fitting the highest, suggesting that the disassembly of the multilayer films follows as a pseudo-second order process. From the plots of *1/A* vs. *time*, the slopes were calculated that correspond to a rate of disassembly for each zone (light vs. dark), and these rates of disassembly of each zone were normalized to each other, for a 'relative rate' ratio of disassembly (RRD). Figure 7B shows the *1/A* vs. *time* plot of PAH-AMA for light/irradiated region (blue points) vs. dark/non-irradiated (red points), which shows a linear slope for the irradiated region. The rate of disassembly of the light region was calculated to be 0.04 A units h^{-1}, compared to the dark region rate of 0.0007 A units h^{-1}, which in this case can be considered to be essentially zero, similar to the small loss of azo from the films by washing for so long in a constant flow of water. This analysis returned a RRD ratio of 57:1for the PAH-AMA films, and results for other polymer-azo dye systems are presented in the SI (Supplementary Figure S2–4A). For the PAH-ALR system the RRD was calculated to be 14:1, and 6:1 for the PAA-BBY system. Several factors that could be influencing the RRD were investigated, as discussed in the following paragraphs.

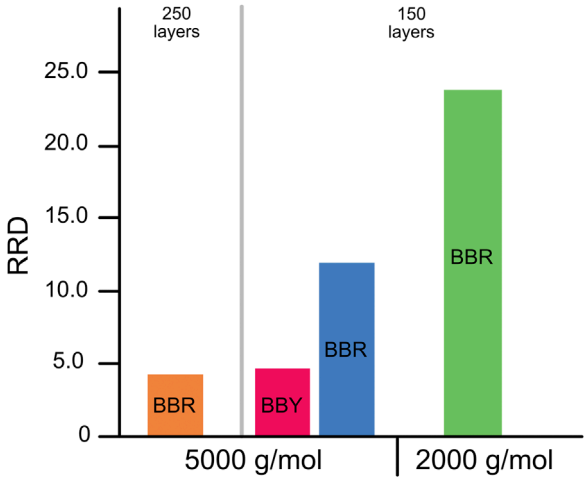

FIGURE 8
Comparison of RRD of multilayer films PAA of different molecular weights with BBR and BBY.

To investigate the role of molecular weight of the polymer used, we compared the disassembly rates of multilayer films made from bismarck brown dyes and monodisperse PAA of molecular weights 2k and 5k. The results (Figure 8, green and blue bars) showed that the 2.5-fold decrease molecular weight of PAA resulted in a 2-fold increase in RRD. Also shown in Figure 8 (orange and the blue bars) is that multilayer films with higher number of layers disassemble more slowly.

To investigate the effect of the structure of the azo dye, two cationic azos were used in our study of PAA: BBY and BBR, which differ structurally only in the addition of three methyl groups in ortho- and para-positions relative to the azo-group in the case of

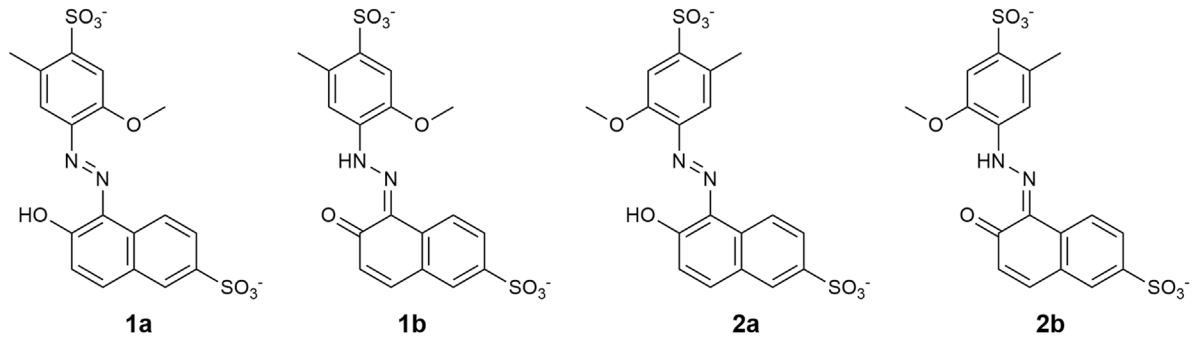

FIGURE 9
Conformational structures of *trans* ALR in the enol **(A)** and keto **(B)** tautomeric form investigated by the DFT method at the B3LYP-D3BJ/ma-def2-TZVP level. The corresponding *cis* isomer of each structure was obtained by rotating the geometry about the azo bond, and then reoptimizing the resultant structure.

TABLE 1 Relative Gibbs free energy, ΔG, at 298.15 K of significant *cis*-ALR and *trans*-ALR conformers with respect to the lowest-energy conformer for both isomers, 2b.

Conformer	ΔG at 298.15 K (kJ/mol)	
	cis-ALR	*trans*-ALR
1a	6.04	23.83
1b	15.84	8.45
2a	0.50	17.80
2b	0.00	0.00

BBR (Figure 2B). A higher RRD was observed for BBR than BBY (Figure 8, blue and red bars). This might be explained by increased electrostatic repulsion between additional methyl groups in the case of BBR leading to less adhesion within multilayer films which gives a greater effect from *trans*-to-*cis* isomerization.

Computational investigation of ALR isomerization

Transitioning from using fabric azo dyes such as BBY and BBR, to low-toxicity azo food dyes such as ALR and AMA has the advantage of creating systems with lower environmental impact, yet this introduces a problem for experimental spectroscopic confirmation of the *trans*-to-*cis* isomerization. A hallmark of most of these low-toxicity azo food dyes is that they generally contain a hydroxy-group in ortho ring position with respect to the azo-group, and this leads to exceedingly fast thermal *cis*-to-*trans* isomerization times in the millisecond to sub-millisecond timescale (Gabor and Fischer, 1962; Ball and Nicholls, 1985; García-Amorós et al., 2010). Unlike BBY and BBR, for example, where the half-life of the *cis* form is on the order of seconds and so is easily confirmed and characterized with accessible laboratory spectroscopic equipment (Edwards et al., 2023), such measurements are precluded for ALR and AMA with recourse only from cold temperatures or ultra-fast flash photolysis techniques. It is speculated that the ortho-hydroxy group enables an azo-hydrazone tautomeric equilibrium, wherein transfer of a proton from the hydroxy group to the azo-group results in reduction of double-bond character, leading to a facile and rapid low-energy rotational transition back to the *trans* form (García-Amorós et al., 2010; García-Amorós and Velasco, 2012; Bandara and Burdette, 2012; Poutanen et al., 2018). Such azo-hydrazone tautomerism has been reported in phenylazonaphthol derivatives similar to ALR and AMA (Özen et al., 2007; Rauf et al., 2015; Vannucci et al., 2021). Indeed, this is likely the very reason that food dyes include this ortho-hydroxy *cis*-eliminator group, as with no significant *cis* concentration for any appreciable duration, FDA approval for use and sale could be sought and obtained for the stable and testable *trans* form only (Gudelj et al., 2011). The *cis* form still does get created on isomerization, even if short-lived, exhibiting rapid thermal isomerization rates due to this azo-hydrazone equilibrium, so applications of azo as a geometric trigger such as what is being described here still work even if spectroscopic confirmation and characterization is too fast to observe.

In lieu of experimental spectroscopy, theoretical analysis of such food dyes can be undertaken. Very few computational studies on azobenzene food dyes have been published, and among these publications, theoretical investigations of the isomerization mechanism still remain unexplored. To support the results presented herein for the isomerization-induced disassembly of LbL films, a theoretical investigation of the isomerization of ALR was carried out using DFT approaches, as a representative system for the large class of ortho-hydroxy azobenzene food dyes. In a recent experimental and DFT study, the acid-base characteristics of ALR were investigated. This study revealed five acid-base forms for ALR, where the form deprotonated at the azo-group and sulphonate groups (Figure 2B) was predicted to be the predominant species at neutral pH (Bevziuk et al., 2017), the pH range relevant to ALR in the context of LbL films presented here. Accordingly, this acid-base form was the focus of all DFT computations discussed next.

All possible conformers of the enol and keto tautomers of *trans*- and *cis*-ALR were investigated. Salient conformers are shown in

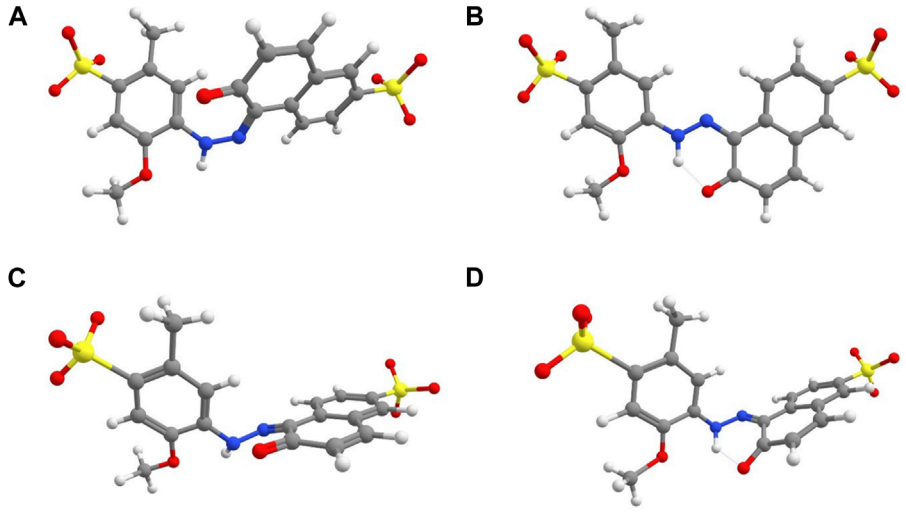

FIGURE 10
Optimized geometries of conformer **2b** of **(A)** *cis*-ALR and **(B)** *trans*-ALR, as well as the rotational transition state for an initial stationary point of **(C)** *cis*-ALR or **(D)** *trans*-ALR. Dotted lines signify hydrogen-bonding.

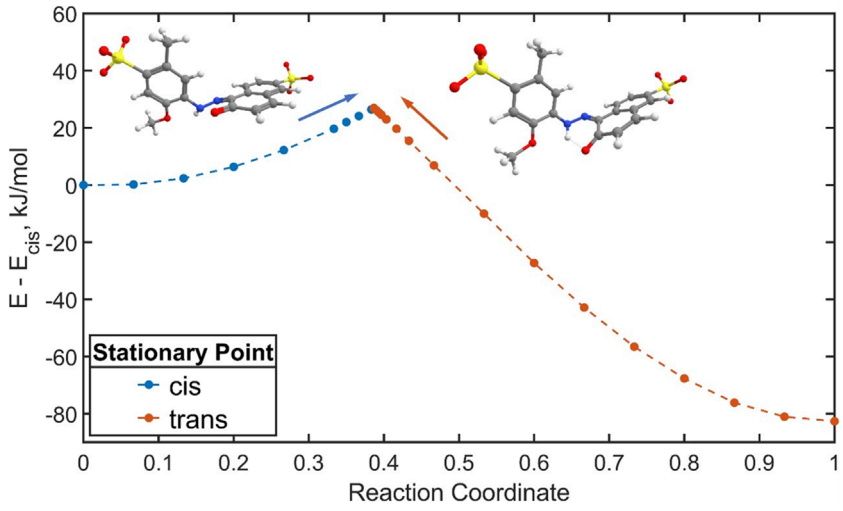

FIGURE 11
Energy profile for *cis*-*trans* thermal isomerization of ALR through the rotation pathway plotted as a function of the normalized reaction coordinate. Data points in blue and red signify *cis* or *trans* isomers as initial stationary points in the geometry scan, respectively. Overlaid structures are the transition states starting from each stationary point.

Figure 9, where the labels **a** and **b** signify the enol and keto forms, respectively. As a note on nomenclature, hydrazone-type molecules can adopt a naming convention different from that of azobenzene, where '*cis*' and '*trans*' no longer refer to configuration about the azo bond. For simplicity and consistency here however, '*trans*' and '*cis*' are used to refer to the ring arrangement about the azo bond only, for all structures considered. Conformer **2b** of both the *trans* and *cis* isomers was identified as the global minimum structure. This finding was expected for the *trans* isomer since a favourable hydrogen bond exists between the tautomeric oxygen and the nearby azo lone pair, as well as additional stabilization through the electrostatic interaction between the methoxy group and tautomeric azo hydrogen. All other possible conformers not shown in Figure 9 were excluded from further analysis since they presented electronic energy barriers of 40–80 kJ/mol relative to conformer **2b.** Table 1 lists ΔG values predicted at 298.15 K for conformers shown in Figure 9, relative to the lowest energy conformer **2b**. Assuming a Boltzmann distribution of these conformers and noting that each *cis* conformer has a 2-fold degeneracy, the calculated isomerization energy ΔG_{iso} at 298.15 K for ALR was 85.9 kJ/mol.

Calculated lowest-energy structures for the keto *trans* and *cis* isomers were stabilized by ketone resonance, which not only

tends to eliminate charge separation of the zwitterionic keto form, but also reduces the double-bond character of the azo-group. As a result, the thermal isomerization process likely obeys a rotation mechanism similarly to azo dyes exhibiting azo-hydrazone tautomerism discussed previously, as well as push-pull azo dyes (García-Amorós et al., 2010; Bandara and Burdette, 2012). The structure of the rotational transition state is shown in Figures 10C, D alongside structures of global minimum *cis* and *trans* geometries in Figures 10A, B. Interestingly, the geometry scan along the CNNC dihedral yielded different transition state structures degenerate in energy depending on whether the initial stationary point was the *cis* isomer (Figure 10C) or the *trans* isomer (Figure 10D). These structures differed by the location of the lone pair on the azo nitrogen adjacent the phenyl ring, as well as the rotation of the phenyl ring with respect to the plane of the azo bond. Animation of the imaginary vibrational modes for both structures revealed an umbrella inversion of the tautomeric azo nitrogen alongside the expected rotation (Supplementary Movies S1, S2). The energy for the transition state was taken as the crossover point in the rotation energy profile shown in Figure 11, which occurred at a dihedral angle of approximately 88°. The cusp appearing in Figure 11 represents a deficiency in the single-reference formulation of Kohn-Sham DFT, which is ill-suited for the description of systems where non-dynamical correlation becomes significant, such as bond breaking. The cusp can be corrected in the spin-flip approach of time-dependent DFT (Shao et al., 2003) which has been recently benchmarked for several azo compounds (Axelrod et al., 2023; Singer et al., 2023). A more thorough investigation will be the subject of a forthcoming separate report for ALR and other similar azobenzene food dyes. Herein, a likely overestimate for the activation free energy barrier $\Delta\mathbf{G}^{\ddagger}$ of ALR thermal isomerization at 298.15 K was found to be 24 kJ/mol, still far lower than the barriers of experimentally observable systems previously reported (Gabor and Fischer, 1962; Ball and Nicholls, 1985; García-Amorós et al., 2010), which suggests a rapid thermal isomerization rate for ALR on the order of microseconds or less. This low barrier may be explained by facile rotation of the hydrazonic *cis* isomer as discussed previously, as well as hydrogen-bonding which tends to stabilize the transition state (Figure 10D) and *trans* isomer (Figure 10B), while being absent in the *cis* isomer. Moreover, Ball and Nicholls found that the isomerization of a related phenylazonaphthol, 4-phenylazo-1-naphthol, incorporated in cellulose triacetate films was accelerated upon introduction of water (Ball and Nicholls, 1985). Wet LbL films in combination with a rapidly isomerizing azo dye such as ALR, likely explains the difficulty for verifying the isomerization process spectroscopically, unless ultrafast flash photolysis techniques are employed.

Conclusion

Multilayer films were assembled by ionic interaction between a series of water-soluble polyions and water-soluble azo dyes, leading to water-insoluble thin films stable to re-dissolution. Upon irradiation with visible light at sunlight wavelengths and intensities however, the films photo-disassembled back to their water-soluble constituent components, via structural photo-isomerization of the azo ionic crosslinkers, with complete recovery of the starting components re-solubilized, unharmed. The relative rate of the disassembly of the films was measured using UV-Vis-spectroscopy, demonstrating that these assemblies can in principle represent fully recyclable (physically, not chemically) degradable materials triggered by exposure to sunlight, with full recovery of starting components. A density functional theory treatment of the allura red azo dye rationalizes the geometrical isomerization mechanism of the photo-disassembly and provides insight into the energetics of the optically-induced structural changes that trigger the disassembly and recovery, as well as why experimental spectroscopic confirmation of the *cis* isomer is prohibitive. We have used the term *disassembly* as opposed to the terms *depolymerization* or *degradation* that are usually used in the literature describing recyclable polymer materials. The term highlights an important property of the multilayer systems developed and reported here, where the constituent components used to make the films are freed by gentle photo-disassembly, allowing recovery and separation from each other, and used again to make new multilayer films, offering a new model system for designing materials with photo-reversible solubility that can be used as fully recyclable and recoverable materials.

Data availability statement

The original contributions presented in the study are included in the article/Supplementary Material, further inquiries can be directed to the corresponding author.

Author contributions

MK: Formal Analysis, Investigation, Software, Visualization, Writing–original draft. CH: Formal Analysis, Investigation, Software, Visualization, Writing–original draft. KE: Conceptualization, Writing–review and editing. TB: Conceptualization, Software, Writing–review and editing. OM: Conceptualization, Funding acquisition, Supervision, Writing–review and editing. WP: Conceptualization, Software, Supervision, Writing–review and editing. CB: Conceptualization, Funding acquisition, Supervision, Writing–review and editing.

Funding

The author(s) declare financial support was received for the research, authorship, and/or publication of this article. This study was financially supported by the Natural Sciences and Engineering Research Council of Canada (NSERC).

Acknowledgments

We also thank the Canada First Research Excellence Fund, for grants to York University through both VISTA (CFREF-2015-00013) and Connected Minds (CFREF-2022-00010) programs.

Conflict of interest

The authors declare that the research was conducted in the absence of any commercial or financial relationships that could be construed as a potential conflict of interest.

Publisher's note

All claims expressed in this article are solely those of the authors and do not necessarily represent those of their affiliated organizations, or those of the publisher, the editors and the reviewers. Any product that may be evaluated in this article, or claim that may be made by its manufacturer, is not guaranteed or endorsed by the publisher.

Supplementary material

The Supplementary Material for this article can be found online at: https://www.frontiersin.org/articles/10.3389/fmats.2024.1334863/full#supplementary-material

References

Axelrod, S., Shakhnovich, E., and Gómez-Bombarelli, R. (2023). Thermal half-lives of azobenzene derivatives: virtual screening based on intersystem crossing using a machine learning potential. *ACS Cent. Sci.* 9 (2), 166–176. doi:10.1021/acscentsci.2c00897

Ayer, M. A., Simon, Y. C., and Weder, C. (2016). Azo-containing polymers with degradation on-demand feature. *Macromolecules* 49 (8), 2917–2927. doi:10.1021/acs.macromol.6b00418

Balkenende, D. W. R., Coulibaly, S., Balog, S., Simon, Y. C., Fiore, G. L., and Weder, C. (2014). Mechanochemistry with metallosupramolecular polymers. *J. Am. Chem. Soc.* 136 (29), 10493–10498. doi:10.1021/ja5051633

Ball, P., and Nicholls, C. H. (1985). Photochromism of the azo tautomer of 4-phenyiazo-1-naphthol and its o-methyl ether in solvents and polymer substrates. *Dyes Pigm* 6 (1), 13–25. doi:10.1016/0143-7208(85)80002-4

Bandara, H. M. D., and Burdette, S. C. (2012). Photoisomerization in different classes of azobenzene. *Chem. Soc. Rev.* 41 (5), 1809–1825. doi:10.1039/c1cs15179g

Becke, A. D. (1993). Density-functional thermochemistry. III. The role of exact exchange. *J. Chem. Phys.* 98 (7), 5648–5652. doi:10.1063/1.464913

Benkhaya, S., M'rabet, S., and El Harfi, A. (2020). Classifications, properties, recent synthesis and applications of azo dyes. *Heliyon* 6 (1), e03271. doi:10.1016/j.heliyon.2020.e03271

Bevziuk, K., Chebotarev, A., Snigur, D., Bazel, Y., Fizer, M., and Sidey, V. (2017). Spectrophotometric and theoretical studies of the protonation of allura red AC and ponceau 4R. *J. Mol. Struct.* 1144, 216–224. doi:10.1016/j.molstruc.2017.05.001

Borato, C. E., Leite, F. L., Mattoso, L. H. C., Goy, R. C., Campana Filho, S. P., de Vasconcelos, C. L., et al. (2006). Layer-by-layer films of poly(o-ethoxyaniline), chitosan and chitosan-poly(methacrylic acid) nanoparticles and their application in an electronic tongue. *IEEE Trans. Dielectr. Electr. Insul.* 13 (5), 1101–1109. doi:10.1109/tdei.2006.247838

Borchers, T., Topic, F., Christopherson, J.-C., Bushuyev, O. S., Vainauskas, J., Titi, H. M., et al. (2021). Cold photo-carving of halogen-bonded co-crystals of a dye and a volatile co-former using visible light. *Nat. Chem.* 14 (5), 574–581. doi:10.1038/s41557-022-00909-0

Bykov, D., Petrenko, T., Izsák, R., Kossmann, S., Becker, U., Valeev, E., et al. (2015). Efficient implementation of the analytic second derivatives of Hartree-Fock and hybrid DFT energies: a detailed analysis of different approximations. *Mol. Phys.* 113 (13-14), 1961–1977. doi:10.1080/00268976.2015.1025114

Cao, Z.-Q., and Wang, G.-J. (2016). Multi-stimuli-responsive polymer materials: particles, films, and bulk gels. *Chem. Rec.* 16 (3), 1398–1435. doi:10.1002/tcr.201500281

Carl, N., Müller, W., Schweins, R., and Huber, K. (2019). Controlling self-assembly with light and temperature. *Langmuir* 36 (1), 223–231. doi:10.1021/acs.langmuir.9b03040

Chamas, A., Moon, H., Zheng, J., Qiu, Y., Tabassum, T., Jang, J. H., et al. (2020). Degradation rates of plastics in the environment. *ACS Sustain. Chem. Eng.* 8 (9), 3494–3511. doi:10.1021/acssuschemeng.9b06635

Chinaglia, S., Tosin, M., and Degli-Innocenti, F. (2018). Biodegradation rate of biodegradable plastics at molecular level. *Polym. Degrad. Stab.* 147, 237–244. doi:10.1016/j.polymdegradstab.2017.12.011

Dong, Y., Ruan, Y., Wang, H., Zhao, Y., and Bi, D. (2004). Studies on glass transition temperature of chitosan with four techniques. *J. Appl. Polym. Sci.* 93, 1553–1558. doi:10.1002/app.20630

Dos Santos, D. S., Bassi, A., Rodrigues, J. J., Misoguti, L., Oliveira, O. N., and Mendonça, C. R. (2003). Light-induced storage in layer-by-layer films of chitosan and an azo dye. *Biomacromolecules* 4 (6), 1502–1505. doi:10.1021/bm025754f

Edwards, K., Kim, M., Borchers, T. H., and Barrett, C. J. (2022). Controlled disassembly of azobenzene cellulose-based thin films using visible light. *Mater. Adv.* 3 (15), 6222–6230. doi:10.1039/d2ma00387b

Edwards, K., Pietro, W. J., Mermut, O., and Barrett, C. J. (2023). Optical and computational study of the trans - cis reversible isomerization of the commercial bis-azo dye bismarck brown Y. *Phys. Chem. Chem. Phys.* 25 (7), 5673–5684. doi:10.1039/D2CP05010B

Eisenberg, A., Yokoyama, T., and Sambalido, E. (1969). Dehydration kinetics and glass transition of poly(acrylic acid). *J. Polym. Sci. Part A Polym. Chem.* 7 (7), 1717–1728. doi:10.1002/pol.1969.150070714

Gabor, G., and Fischer, E. (1962). Tautomerism and geometrical isomerism in arylazophenols and naphthols. part II.[1a]2-phenylazo-3-naphthol. the effect of internal hydrogen bonds on photoisomerization.[1b]part I. *J. Phys. Chem.* 66 (12), 2478–2481. doi:10.1021/j100818a037

García-Amorós, J., Sánchez-Ferrer, A., Massad, W. A., Nonell, S., and Velasco, D. (2010). Kinetic study of the fast thermal cis-to-trans isomerisation of para-ortho- and polyhydroxyazobenzenes. *Phys. Chem. Chem. Phys.* 12 (40), 13238–13242. doi:10.1039/c004340k

García-Amorós, J., and Velasco, D. (2012). Recent advances towards azobenzene-based light-driven real-time information-transmitting materials. *Beilstein J. Org. Chem.* 8, 1003–1017. doi:10.3762/bjoc.8.113

Grimme, S., Antony, J., Ehrlich, S., and Krieg, H. (2010). A consistent and accurate *ab initio* parametrization of density functional dispersion correction (DFT-D) for the 94 elements H-Pu. *J. Chem. Phys.* 132, 154104. doi:10.1063/1.3382344

Grimme, S., Ehrlich, S., and Goerigk, L. (2011). Effect of the damping function in dispersion corrected density functional theory. *J. Comput. Chem.* 32, 1456–1465. doi:10.1002/jcc.21759

Gudelj, I., Hrenović, J., Dragičević, T. L., Delaš, F., Soljan, V., and Gudelj, H. (2011). Azo dyes, their environmental effects, and defining a strategy for their biodegradation and detoxification. *Arh. Hig. Rada. Toksikol.* 62 (1), 91–101. doi:10.2478/10004-1254-62-2011-2063

Ishikawa, M., Ohzono, T., Yamaguchi, T., and Norikane, Y. (2017). Photo-enhanced aqueous solubilization of an azo-compound. *Sci. Rep.* 7 (1), 6909–7635. doi:10.1038/s41598-017-06947-w

Izsák, R., and Neese, F. (2011). An overlap fitted chain of spheres exchange method. *J. Chem. Phys.* 135 (14), 144105. doi:10.1063/1.3646921

Ji, Y., Oka, M., and Honda, S. (2021). Synthesis of reversibly photocleavable pseudo-ladder polymers. *Polym. Chem.* 12 (32), 4621–4625. doi:10.1039/d1py00646k

Jung, D., Rust, T., Völlmecke, K., Schoppa, T., Langer, K., and Kuckling, D. (2021). Backbone vs. sidechain: two light-degradable polyurethanes based on 6-nitropiperonal. *Polym. Chem.* 12 (31), 4565–4575. doi:10.1039/d1py00442e

Karing, V. A., Kozlov, P. V., and Wan, N.-T. (1960). Investigation of the glass phase transition temperature in cellulose. *Dokl. Akad. Nauk. SSSR* 130, 356–358.

Kean, T., and Thanou, M. (2010). Biodegradation, biodistribution and toxicity of chitosan. *Adv. Drug Deliv. Rev.* 62 (1), 3–11. doi:10.1016/j.addr.2009.09.004

Krogman, K. C., Cohen, R. E., Hammond, P. T., Rubner, M. F., and Wang, B. N. (2013). Industrial-scale spray layer-by-layer assembly for production of biomimetic photonic systems. *Bioinspir. Biomim.* 8 (4), 045005. doi:10.1088/1748-3182/8/4/045005

Landry, M. J., Applegate, M. B., Bushuyev, O. S., Omenetto, F. G., Kaplan, D. L., Cronin-Golomb, M., et al. (2017). Photo-induced structural modification of silk gels containing azobenzene side groups. *Soft Matter* 13 (16), 2903–2906. doi:10.1039/c7sm00446j

Lee, C., Yang, W., and Parr, R. G. (1988). Development of the Colle-Salvetti correlation-energy formula into a functional of the electron density. *Phys. Rev. B Condens. Matter.* 37 (2), 785–789. doi:10.1103/PhysRevB.37.785

Li, X., Liu, D., Wang, Y., Xu, S., and Liu, H. (2018). Water dispersive upconversion nanoparticles for intelligent drug delivery system. *Colloids Surf. A Physicochem. Eng. Asp.* 555, 55–62. doi:10.1016/j.colsurfa.2018.06.036

Ma, L., Baumgartner, R., Zhang, Y., Song, Z., Cai, K., and Cheng, J. (2015). UV-responsive degradable polymers derived from 1-(4-aminophenyl) ethane-1,2-diol. *J. Polym. Sci. Part A Polym. Chem.* 53 (9), 1161–1168. doi:10.1002/pola.27550

Neese, F. (2012). The ORCA program system. *WIREs Comput. Mol. Sci.* 2 (1), 73–78. doi:10.1002/wcms.81

Neese, F. (2017). Software update: the ORCA program system, version 4.0. *WIREs Comput. Mol. Sci.* 8, e1327. doi:10.1002/wcms.1327

Neese, F., Wennmohs, F., Becker, U., and Riplinger, C. (2020). The ORCA quantum chemistry program package. *J. Chem. Phys.* 152 (22), 224108. doi:10.1063/5.0004608

Neese, F., Wennmohs, F., Hansen, A., and Becker, U. (2009). Efficient, approximate and parallel Hartree–Fock and hybrid DFT calculations. A 'chain-of-spheres' algorithm for the Hartree–Fock exchange. *Chem. Phys.* 356 (1-3), 98–109. doi:10.1016/j.chemphys.2008.10.036

Özen, A. S., Doruker, P., and Aviyente, V. (2007). Effect of cooperative hydrogen bonding in azo-hydrazone tautomerism of azo dyes. *J. Phys. Chem. A* 111 (51), 13506–13514. doi:10.1021/jp0755645

Perkasa, D. P., Erizal, E., Darmawan, D., and Rasyid, A. (2013). Effect of gamma irradiation on mechanical and thermal properties of fish gelatin film isolated from lates calcarifer scales. *Indones. J. Chem.* 13, 28–35. doi:10.22146/ijc.21322

Poutanen, M., Ahmed, Z., Rautkari, L., Ikkala, O., and Priimagi, A. (2018). Thermal isomerization of hydroxyazobenzenes as a platform for vapor sensing. *ACS Macro Lett.* 7 (3), 381–386. doi:10.1021/acsmacrolett.8b00093

Rauf, M. A., Hisaindee, S., and Saleh, N. (2015). Spectroscopic studies of keto-enol tautomeric equilibrium of azo dyes. *RSC Adv.* 5 (23), 18097–18110. doi:10.1039/C4RA16184J

Roberts, G. A. F. (1992). "Structure of chitin and chitosan," in *Chitin chemistry* (London, UK: Red Globe Press London), 1–53. doi:10.1007/978-1-349-11545-7_1

Santos, D. S. d., Bassi, A., Misoguti, L., Ginani, M. F., Oliveira, O. N. d., and Mendonça, C. R. (2002). Spontaneous birefringence in layer-by-layer films of chitosan and azo dye sunset yellow. *Macromol. Rapid Commun.* 23 (16), 975–977. doi:10.1002/1521-3927(200211)23:16<975::aid-marc975>3.0.co;2-w

Shao, Y., Head-Gordon, M., and Kyrlov, A. I. (2003). The spin-flip approach within time-dependent density functional theory: theory and applications to diradicals. *J. Chem. Phys.* 118 (11), 4807–4818. doi:10.1063/1.1545679

Shellenberger, M. (2020). *Apocalypse never: why environmental alarmism hurts us all*. New York, NY: Harper.

Si, J., Yang, X., Luan, H., Shao, Y., and Yao, K. (2021). Cheap, fast and durable degradation of azo dye wastewater by zero-valent iron structural composites. *J. Environ. Chem. Eng.* 9 (5), 106314. doi:10.1016/j.jece.2021.106314

Silva, M. M., Reboredo, F. H., and Lidon, F. C. (2022). Food colour additives: a synoptical overview on their chemical properties, applications in food products, and health side effects. *Foods* 11 (3), 379. doi:10.3390/foods11030379

Singer, N. K., Schlögl, K., Zobel, J. P., Mihovilovic, M. D., and González, L. (2023). Singlet and triplet pathways determine the thermal Z/E isomerization of an arylazopyrazole-based photoswitch. *J. Phys. Chem. Lett.* 14 (40), 8956–8961. doi:10.1021/acs.jpclett.3c01785

Siti Mohd Binti Isa, A., and Mohamed, R. (2015). Physical and mechanical properties of chitosan and Polyethylene blend for food packaging film. *Int. J. Mech. Prod. Eng.* 3 (10), 51–55.

Szcześniak, L., Rachocki, A., and Tritt-Goc, J. (2007). Glass transition temperature and thermal decomposition of cellulose powder. *Cellulose* 15, 445–451. doi:10.1007/s10570-007-9192-2

Tay, S. Y., Wong, V. L., Lim, S. S., and Teo, I. L. R. (2020). Adsorption equilibrium, kinetics and thermodynamics studies of anionic methyl orange dye adsorption using chitosan-calcium chloride gel beads. *Chem. Eng. Commun.* 208 (5), 708–726. doi:10.1080/00986445.2020.1722655

Tong, X., Qiu, Y., Zhao, X., Xiong, B., Liao, R., Peng, H., et al. (2019). Visible light-triggered gel-to-sol transition in halogen-bond-based supramolecules. *Soft Matter* 15 (31), 6411–6417. doi:10.1039/c9sm01310e

Vannucci, G., Cañamares, M. V., Prati, S., and Sanchez-Cortes, S. (2021). Analysis of the tautomeric equilibrium of two red monoazo dyes by UV-Visible, Raman and SERS spectroscopies. *Spectrochim. Acta A.* 261, 120007. doi:10.1016/j.saa.2021.120007

Wang, Z., and Liao, Y. (2016). Reversible dissolution/formation of polymer nanoparticles controlled by visible light. *Nanoscale* 8 (29), 14070–14073. doi:10.1039/c6nr02163h

Weigend, F. (2002). A fully direct RI-HF algorithm: implementation, optimised auxiliary basis sets, demonstration of accuracy and efficiency. *Phys. Chem. Chem. Phys.* 4 (18), 4285–4291. doi:10.1039/B204199P

Weigend, F. (2006). Accurate Coulomb-fitting basis sets for H to Rn. *Phys. Chem. Chem. Phys.* 8 (9), 1057–1065. doi:10.1039/B515623H

Weigend, F., and Ahlrichs, R. (2005). Balanced basis sets of split valence, triple zeta valence and quadruple zeta valence quality for H to Rn: design and assessment of accuracy. *Phys. Chem. Chem. Phys.* 7 (18), 3297–3305. doi:10.1039/B508541A

Winch, P. (2020). Recycling was a lie — a big lie — to sell more plastic, industry experts say | CBC Documentaries. CBC. Available at: https://www.cbc.ca/documentaries/the-passionate-eye/recycling-was-a-lie-a-big-lie-to-sell-more-plastic-industry-experts-say-1.5735618.

Wunsch, J. R. (2000). *Polystyrene: synthesis, production and applications. Shawbury*. Shrewsbury, Shropshire, UK: Rapra Technology Ltd.

Xue, P., Ding, J., Jin, M., and Lu, R. (2017). Rapid gel-to-sol transition triggered by a photoacid generator under low-power light. *J. Mater. Chem. C.* 5 (22), 5299–5303. doi:10.1039/c7tc01028a

Yang, S., Li, N., Chen, D., Qi, X., Xu, Y., Xu, Y., et al. (2013). Visible-light degradable polymer coated hollow mesoporous silica nanoparticles for controlled drug release and cell imaging. *J. Mater. Chem. B.* 1 (36), 4628–4636. doi:10.1039/c3tb20922a

Yu, Z., Ma, L., Ye, S., Li, G., and Zhang, M. (2020). Construction of an environmentally friendly octenylsuccinic anhydride modified pH-sensitive chitosan nanoparticle drug delivery system to alleviate inflammation and oxidative stress. *Carbohyr. Polym.* 236, 115972. doi:10.1016/j.carbpol.2020.115972

Zheng, J., Xu, X., and Truhlar, D. G. (2011). Minimally augmented Karlsruhe basis sets. *Theor. Chem. Acc.* 128, 295–305. doi:10.1007/s00214-010-0846-z

Zhu, X., Chen, J., Hu, Y., Zhang, N., Fu, Y., and Chen, X. (2021). Tuning complexation of carboxymethyl cellulose/cationic chitosan to stabilize Pickering emulsion for curcumin encapsulation. *Food Hydrocoll.* 110, 106135. doi:10.1016/j.foodhyd.2020.106135

Zrimec, J., Kokina, M., Jonasson, S., Zorrilla, F., and Zelezniak, A. (2021). Plastic-degrading potential across the global microbiome correlates with recent pollution trends. *mBio* 12 (5), e0215521. doi:10.1128/mbio.02155-21